# New Tropospheric Range Corrections With Seasonal Adjustment

C. C. Chao
*Tracking and Orbit Determination Section*

*A study of two years' radiosonde balloon measurement shows that most of the significant seasonal fluctuations in refractivity profiles are due to the variation of the water content in the troposphere. At each of the six weather stations, the long-term seasonal variation in refractivity profile repeats quite well through the two-year span. Based on the two years' data a new tropospheric range calibration method using monthly mean parameters at each station was developed.*

*The uncertainty of range correction with the new model over one pass is estimated to be 0.30–0.35 m for a 10-deg minimum elevation angle and 0.40–0.50 m for a 6-deg minimum elevation angle. This is below the required accuracy for tropospheric calibration of both Mariner Mars 1971 (MM71) and Viking 1975 missions.*

## I. Introduction

It is our current goal to examine the variations in the refractory profiles in the hope of reducing the uncertainty in range correction with a time-dependent model.

Radio tracking is directly affected by the refraction of the troposphere, and extensive efforts have been devoted to the correction of this error by many researchers. In the past, tropospheric refraction was calibrated with a model which was independent of time. This neglected the possible temporal fluctuations in the refractivity of the troposphere. A recent study of one year's radiosonde balloon data by Ondrasik and Thuleen (Ref. 1) indicated that the tropospheric zenith range effect has a variation of about $\pm 5\%$ of its yearly average. According to Ref. 2, the 5% uncertainty in zenith range effect may cause a greater percentage (6 to 8%) range effect uncertainty at low elevation angles because of the possible variations in the refractivity profile. An 8% uncertainty in range effect corresponds to more than 1 m in the overall uncertainty in range correction over the whole pass, which exceeds the requirement of the MM71 mission ($\sigma\Delta\rho/_{\text{pass}} = \frac{1}{2}$ m, lowest elevation = 10 deg) and the *Viking* 1975 Mission ($\sigma\Delta\rho/_{\text{pass}} = 1$ m, lowest elevation = 6 deg). When the two-station tracking or very long baseline interferometry (VLBI) techniques are employed, the low elevation angle data will become more important, since these long baselines generally result in data being obtained at low elevation angles (Ref. 3). The required uncertainty in range correction over one pass by VLBI is below 1 m, which

cannot tolerate the seasonal fluctuations in refractivity of troposphere.

The new model of tropospheric calibration was developed as a result of the following investigations:

(1) Examination of the seasonal variations in the refractivity profiles based on two years' radiosonde balloon measurement taken at six weather stations near five of the DSN stations.

(2) Comparison of the exponential model that has long been used with the measured profile of refractivity, and the derivation of an analytic expression which can more closely represent the actual dry refractivity profile than the exponential function does.

(3) Estimation of uncertainties of range effect due to the seasonal fluctuations in refractivity profiles found in (1). Examination of the improvement that can be obtained by using the monthly mean profiles.

(4) Development of a new tropospheric calibration model with seasonal adjustment. The zenith range effect is estimated from balloon data combined with prediction from surface measurement derived by Berman.

## II. Refractivity Profiles

The refractivity of the troposphere at a given altitude is commonly determined from the following equation (Ref. 4)

$$N = \frac{77.6}{T} P + \frac{4810e}{T} \tag{1}$$

where

$P$ = pressure, mb

$T$ = temperature, °K

$e$ = vapor pressure, mb

and

$$e = 6.1 \exp_{10}\left(\frac{7.4475\, T_c}{234.7 + T_c}\right)\left(\frac{RH}{100}\right)$$

where

$RH$ = relative humidity, %

$T_c$ = temperature, °C

$\exp_{10} y = 10^y$

The values of $P$, $T$, and $RH$ are the measured data at a given altitude from the radiosonde balloon. An approximation to the errors in $N$ resulting from the use of Eq. (1) due both to the errors in the equation itself and to errors in the meteorological measurements, is given by Bean and Dutton (Ref. 4) as shown in Table 1.

The first and second terms of Eq. (1) will be referred to as the dry and wet refractivity, $N_D$ and $N_W$, respectively.

Because of the seasonal or daily variations of the parameters in Eq. (1), $P$, $T$, and $RH$, the values of $N$ above a station are to have similar types of variations from time to time. The values of dry and wet refractivity, $N_D$ and $N_W$, were calculated from the radiosonde balloon measurements taken at the six stations (Table 2). It is convenient to examine the dry and wet refractivity profiles separately from the two years' data.

### A. Dry Refractivity Profiles

About 90% of the total refractivity, $N$, is due to the dry component in the first 6.1 km (20,000 ft). From there upward, the wet component diminishes and the dry part becomes the total refractivity. From Eq. (1), we can express the dry component refractivity as:

$$N_D = 77.6 \frac{P}{T} \tag{2}$$

The variations in $N_D$ as resulted from the fluctuations in pressure $P$ and temperature $T$ in the troposphere were investigated using the radiosonde balloon measurements taken at six weather stations. The standard deviations of the dry refractivity, $\sigma_{dry}$, from the monthly mean at Edwards AFB were calculated and tabulated in Table 3. The results indicate that $N_D$ has greater deviations at low altitude. Above 6.1 km (20,000 ft), most of the deviations are less than the magnitude of the uncertainties due to measurement of data and Eq. (1) (See Table 1). This implies that the fluctuations of $N_D$ above 6.1 km (20,000 ft) are probably so small in magnitude that the current radiosonde balloon measurement fails to filter it out. In other words, the density of the troposphere above 6.1 km (20,000 ft) stays fairly constant. The variations of the monthly mean of $N_D$ at various altitudes were also shown in Table 3. The fluctuation in $N_D$ below 6.1 km (20,000 ft) is caused by the daily and seasonal variations in pressure and temperature resulting from the weather change in the area. As it will be shown later, the magnitude of these low-altitude fluctuations is less than the magnitude of the fluctuations of the wet component. Since the dry component

of refractivity dominates the total refraction and is relatively steady in most portions of the troposphere, an analytic expression for mapping the range effect down to lower elevation angles may be derived.

If we assume the atmosphere is in static equilibrium, spherically symmetrical and obeys the perfect gas law, then we can write the governing equations for the dry part as Berman did in Ref. 7.

$$-\rho g = \frac{dP}{dr} \tag{3}$$

$$P = \rho RT \tag{4}$$

where $P$, $\rho$, and $T$ are functions of $r$ only, and

$\rho$ = density of air

$P$ = pressure

$T$ = absolute temperature

$r$ = geocentric distance

$R$ = gas constant

$g$ = gravitational acceleration

The temperature profile, $T(r)$ in the atmosphere depends on the thermal property of the atmosphere and the heat balance of the Earth. According to the measured data from the U.S. Standard Atmosphere Supplements, 1966, the temperature profiles in the troposphere can be classified into two types; linearly decreasing up to about 10 km and then remain fairly constant up to 30 km (Fig. 1).

$$T \cong T_0 - \gamma (r - r_0) \qquad r_0 < r < r_m \tag{5}$$

$$T \cong T_m \qquad r_m < r < r_{\text{tropo}} \tag{6}$$

where

$\gamma$ = temperature lapse rate

$r_0$ = surface altitude

$r_m$ = altitude where temperature becomes constant with altitude

$r_{\text{tropo}}$ = outer edge of troposphere (about 40 km)

Then we can combine Eqs. (3), (4), (5) and (6) and integrate to get

$$P = P_0 \left(1 - \frac{\gamma h}{T_0}\right)^{\alpha} \tag{7}$$

$$P = P_m \exp\left[-\frac{g}{RT_m}(h - h_m)\right] \tag{8}$$

where $\alpha = g/\gamma R$, $h = r - r_0$, $P_m, T_m$ are the values of $P$ and $T$ at $r_m$, $P_0$, $T_0$ are conditions at $r_0$. Substituting Eqs. (7) and (8) into the dry part of Eq. (1), we obtain the expression for dry refractivity profile:

$$N_D = \frac{77.6}{T} P = 77.6 \frac{P_0 \left(1 - \frac{\gamma h}{T_0}\right)^{\alpha}}{T_0 \left(1 - \frac{\gamma h}{T_0}\right)}$$

$$= N_{D0} \left(1 - \frac{\gamma h}{T_0}\right)^{\alpha - 1} \tag{9}$$

$$N_D = \frac{77.6}{T_m} P_m \exp\left[-\frac{g}{RT_m}(h - h_m)\right]$$

$$= N_{Dm} \exp\left[-\frac{g}{RT_m}(h - h_m)\right] \tag{10}$$

where

$N_{D0}$ = dry surface refractivity

$N_{Dm}$ = dry refractivity at $r_m$

The profile in the first 10 km follows a polynomial of power $\alpha - 1$, that in the next 20 km decays exponentially under an approximately isothermal condition. The average value of $\alpha - 1$, based on the mean temperature profiles shown in Fig. 1, is about 4. This explains why a quartic profile as suggested by Hopfield (Ref. 5) has closer agreement with the data than a simple exponential profile does in the first 12.2 km (40,000 ft) (Fig. 2). The quartic model deviates by an appreciable amount when it is higher than 15.2 km (50,000 ft) where a second stage exponential model works nicely as shown in Fig. 3.

### B. Wet Refractivity Profiles

As indicated in Ref. (1), the dominant error source in the zenith range tropospheric correction computed from radiosonde data comes from the variations in the wet

component of refractivity, $N_W$. It can be rewritten in the following way:

$$N_W = 3.733 \times 10^5 \frac{e}{T^2} \tag{11}$$

or

$$N_W = 2.277 \times 10^4 \frac{RH}{T^2} \exp_{10}\left(\frac{7.4475\, T_c}{234.7 + T_c}\right) \tag{12}$$

The value of the wet component of refractivity $N_W$ is directly proportional to the water content in the troposphere. Equation (12) indicates that changes in temperature and relative humidity will cause variations in the values of $N_W$. As shown in Table 4, the value of $N_W$ varies drastically when weather changes. The variation in relative humidity is a complicated function of the local weather nature, and thus it is very difficult to approximate the profile of $N_W$ analytically as a function of altitude similar to the dry component $N_D$.

According to the balloon data, the wet refractivity profiles are confined within the first 6.1 to 7.6 km (20,000 to 25,000 ft) of altitude where most of the water vapor in the atmosphere is contained. The temperature and relative humidity for a particular area are known to have both daily and seasonal variations, thus the wet refractivity $N_W$ computed from Eq. (12) should also have two types of variations.

### *1. Daily (short-term) fluctuations*

The typical diurnal temperature change is around 10 to 15°C at the Goldstone DSCC, and the change in relative humidity is 20 to 25%. Thus from Table 4 the corresponding change in $N_W$ will be around 10 to 20 units, which may lead to a significant change in range effect.

The actual daily fluctuations in the wet component, $N_W$, can be found from the computed data from radiosonde balloon measurements. Figures 4 and 5 show the profiles of $N_W$ above a meteorological station for the first 6.1 km (20,000 ft), where $N_W$ is significant. Due to the limitation of space, only the summer and winter type profiles are shown in these figures.

The three stations in the northern hemisphere, Edwards Air Force Base in California, Yucca Flats in Nevada, and Madrid in Spain, have very different types of profiles between summer and winter. About ten days' data in January plotted in Fig. 4 reveals the average low profiles and lesser daily fluctuations in winter. While the corresponding plot (Fig. 5) shows that the summer weather makes the wet component of refractivity very active and fluctuating. The profiles in the rest of the year fall between these two types of profiles, and they will be seen on the monthly mean profiles later.

The other three stations in the southern hemisphere, Woomera and Wagga in Australia, and Pretoria in South Africa, show similar characteristics in the summer and winter type of profiles except that the fluctuations in winter (June–August) are more active than that of the northern hemisphere stations.

### *2. Long-term (seasonal) fluctuations*

The monthly mean of the wet refractivity profiles for stations at Edwards Air Force Base and Madrid were plotted in Figs. 6 and 7. The seasonal variations can be easily seen from those monthly mean profiles. The summer type profiles are consistently the highest of the year, while the winter type profiles are the lowest. The magnitude of the total variation in a year and the shape of the average profiles varies from station to station due to the particular local weather variation. For instance, the magnitude of variations at Edwards Air Force Base is greater than that at Madrid, and the former has a peculiar type of profile in the low altitude where a maximum usually occurs at a height of about 1000 ft above the surface. It should be noticed that the magnitudes of short-term fluctuations in winter, spring, and fall are generally several times smaller than those of the long-term fluctuations. In the summer, the short-term fluctuation becomes so active that it is almost equal to the long term in magnitude. The range of standard deviations from the monthly mean were shown in Table 5. It has higher deviations than the dry part.

It is also important to examine the repeatability of the seasonal variations at each station. Thuleen and Ondrasik[1] recently made a comparison of the two-year zenith range effects at the six weather stations, and the results showed good repeatability of the seasonal variations at each station. The results of this analysis also indicate that the seasonal variations in the shape of both dry and wet profiles repeat quite well based on the two years' data. Figures 4 and 5, and 8 and 9 give a sample of the wet refractivity profiles in the same months of the two years. Their agreement is generally good. The difference between the two years data are of the same magnitude as that of the

[1] "The Repetition of Seasonal Variations in the Tropospheric Zenith Range Effect," in this issue.

short-term fluctuations. This gives us confidence in that a new calibration model with seasonal adjustment can significantly reduce the uncertainties in range and range rate calibrations caused by seasonal fluctuations.

## III. Uncertainty of Range Effect Due to Seasonal Fluctuations at Various Elevation Angles

Since the range and range rate correction for the troposphere are directly derived from the profiles of refractivity, $N$, any change in $N$ will eventually affect the precision of a fixed-profile calibration model for the troposphere in radio tracking. An estimation is made here to reflect the uncertainties in range correction for troposphere caused by the fluctuations in the profiles of refractivity obtained from radiosonde balloon measurement. Table 6 shows the average uncertainties ($1\sigma$) in range correction at various elevation angles of a fixed calibration model (2-year mean) and a seasonally adjusted model (monthly mean). Values in Table 6 were computed by a ray trace program.

It is seen that the fixed model based on the two-year mean profile at each station has an uncertainty of about 0.11 m (5%) at zenith and 1.6 m (6.5%) at 5 deg of elevation angle. When the monthly mean profiles are used, the uncertainty in the range correction has been reduced by almost a factor of three. The greatest part of the uncertainty is due to the fluctuations in the wet component. The values at zenith as shown in Table 6 seem to agree with the results in Ref. 1.

## IV. Range Correction Combined With Surface Measurement

It is expected that frequent radiosonde balloon measurements will reduce the uncertainty due to temporal fluctuations. However, it is not practically possible to take balloon measurement as frequently as one desires, say once every hour. Thus the method for predicting the profiles and zenith range effect through surface measurement which can be taken frequently or even continuously becomes very helpful.

Recently Berman (Ref. 6) derived a set of formulas which can predict the dry and wet component of the zenith range effect from ground surface measurement.

$$\Delta\rho_{Z\,\mathrm{dry}} = 2.276\,P_0 \tag{11}$$

$$\Delta\rho_{Z\,\mathrm{wet}} = 0.566\frac{(RH)}{\gamma}\left(1-\frac{c}{T_0}\right)^2 \exp\left(\frac{AT_0-B}{T_0-C}\right) \tag{12}$$

where

$\Delta\rho_Z$ = zenith range correction, m

$P_0$ = surface pressure, bar

$\gamma$ = temperature lapse rate, K/km

$T_0$ = linearly extrapolated surface temperature, K

$(RH)_0$ = surface relative humidity $(0 \leq (RH)_0 \leq 1)$

$A = 17.1486$

$B = 4684.1331$

$C = 38.45$

Equation (11) is obtained under the assumption of static equilibrium, perfect gas of the troposphere and constant gravitation acceleration, $g$. If these assumptions are true, Eq. (11) has the potential to be able to predict the dry zenith range effect with an uncertainty of $\pm 2$ mm for a precision of $\pm 1$ mb in surface pressure measurement (Ref. 7). According to Ref. 6, the uncertainty of the wet zenith range effect computed from Eq. (12) is 2.8 cm ($1\sigma$). Thus the total zenith range effect can be predicted from surface measurement with, potentially, the same accuracy as radiosonde measurement. Two of the four parameters $P_0$, and $(RH)_0$ can be measured continuously at each tracking station; for example, the micro-barograph measures surface pressure continuously.

The temperature lapse rate $L$ and $T_0$ can be estimated from less frequent (perhaps every several days or use monthly mean) radiosonde measurement. Another advantage of Eq. (11) is that it gives the dry zenith range effect of the entire troposphere, while most of the radiosonde balloon data end at about 24.4 km (80,000 ft), and the contribution due to rest of the troposphere has to be estimated. Besides, the balloon, instead of ascending along zenith direction, may fly along a 30- to 45-deg elevation due to local wind. Equation (12) is derived under the assumption of constant $RH$, when $RH$ varies drastically with altitude, the wet zenith range effect should be obtained directly from radiosonde measurement. Once the zenith range correction is accurately determined, the next

step is to map it down to lower elevation angles by employing a correct refractivity profile.

A cursory examination of the sensitivity of the tropospheric range effect to the shape of the refractivity profile has been made in Ref. 2. It indicates that for a slight variation in the profile of refractivity, the effect on the ratio of mapping zenith range effect to lower elevation is very small. According to measured data (Table 3), the variations in the shape of the dry refractivity profile is insignificantly small for most of the troposphere. Thus a mean profile closely approximating the real data can be obtained for generating a standard table to map the dry zenith range error down to 3 deg elevation angle within 3% uncertainty. After fitting the measured data with the previously derived function (Eqs. 9 and 10), a best-fit profile for the dry part refractivity is found.

$$N_{\text{dry}} = 269\left(1 - \frac{h}{42.7}\right)^4 \qquad h \leq 12.2\,\text{km} \qquad (13)$$

$$N_{\text{dry}} = 70\exp\left[-\frac{(h - 12.2)}{6.4}\right] \qquad h \geq 12.2\,\text{km} \qquad (14)$$

Although the wet profiles were found varying drastically from time to time, most of them seem to have similar monotonically decreasing shape (Figs. 4 and 5). They can be approximated by the following expression without loss of significant accuracy, if the deviations in shape are not too great.

$$N_{\text{wet}} = N_s\left(1 - \frac{h}{13}\right)^4 \qquad h \leq 13\,\text{km} \qquad (15)$$

$$N_{\text{wet}} = 0 \qquad h \geq 13\,\text{km} \qquad (16)$$

In case of bad weather, when the shape of the profile from special balloon measurement is significantly different from the quartic profile of Eq. (15), a special ray tracing should be made for the mapping.

The above calibration which based on Berman's formula for zenith range correction from monthly mean parameters, and the mapping table for range correction at lower elevation angles was adopted as the new model for tropospheric correction in DPODP for the *Mariner* Mars 1971 Mission. The values of the monthly means of the four parameters in Berman's formulas calculated from the two years' data and the standard mapping table can be found in Ref. 8.

The past time-independent model in DPODP assumes that the refractivity decreases exponentially with height above sea level. Based on the specified profile ($N = 340\exp[-h/7]$) two empirical formulas were fitted to give the range correction at any elevation angle.

$$\Delta\rho = 1.8958\,\frac{N}{340}(\sin\gamma + 0.06483)^{-1.4} \qquad (17)$$

$$\Delta\rho = \frac{2.6}{\sin\gamma + 0.015}\,\frac{N}{340} \qquad (18)$$

The two formulas, Eq. (17) and Eq. (18), were originated from D. Cain. The second equation is a modified function for better results when the elevation is 15 deg or higher. The zenith range effect computed from the two formulas with the recommended values of total surface refractivity $N$ at each station were shown and compared with measurements in Table 7. The values computed from Eq. (17) are almost 1 m lower than the average values from radiosonde balloon measurement. The corresponding uncertainties in range correction over a symmetrical path were estimated (Ref. 9) and are shown in Table 8. The new seasonally adjusted (monthly mean) calibration model can almost reduce the range correction uncertainty over a pass by one order of magnitude.

Recently, B. Winn (Ref. 10) has compared the old and new methods by applying them to calibrate the real tracking data, and the preliminary results already showed significant improvement of the new monthly mean model.

## V. Conclusion

A study of two years' radiosonde balloon measurement shows that most of the significant seasonal fluctuations in refractivity profiles which occur in the first 7.6 km (25,000 ft) are due to the variation of the water content in that portion of the troposphere. At each of the six weather stations, the long term seasonal variation in refractivity profile repeats quite well through the two-year span.

An analytic expression which can more closely represent the actual dry refractivity profile than the exponential function has been derived. The wet refractivity profile is approximated by a simple quartic equation. The uncertainties in range correction using a monthly mean profile were found in only 40 of the uncertainties in range effect with a 2-yr mean profile.

A new tropospheric calibration model with seasonal adjustment was developed, based on the monthly parameters obtained from the two-year radiosonde balloon

measurement combined with surface prediction. The uncertainty of range correction with the new model over one symmetrical pass is estimated to be 0.30 to 0.35 m for a 10-deg minimum elevation angle and 0.40 to 0.50 m for a 6-deg minimum elevation angle. This is below the required accuracy of both MM'71 and *Viking* 1975 missions.

## Acknowledgment

The author would like to thank Kathryn L. Thuleen for supplying the computed refractivity from radiosonde balloon measurement and Nancy Hamata for her assistance in programming for making the necessary plots.

## References

1. Ondrasik, V. J., and Thuleen, K. L., "Variations in the Zenith Tropospheric Range Effect Computed From Radiosonde Balloon Data," in *The Deep Space Network*, Space Programs Summary 37-65, Vol. II, pp. 25–35. Jet Propulsion Laboratory, Pasadena, Calif., Sept. 30, 1965.
2. Miller, L. F., Ondrasik, V. J., and Chao, C. C., "A Cursory Examination of the Sensitivity of the Tropospheric Range and Doppler Effects to the Shape of the Refractivity Profile," in *The Deep Space Network Progress Report*, Technical Report 32-1526, Vol. I, pp. 22–30. Jet Propulsion Laboratory, Pasadena, Calif.
3. Williams, J. G., "Very Long Baseline Interferometry and Its Sensitivity to Geophysical and Astronomical Effects," in *The Deep Space Network*, Space Programs Summary 37-62, Vol. II, pp. 49–55. Jet Propulsion Laboratory, Pasadena, Calif., March 31, 1970.
4. Bean, B. R., and Dutton, E. J., "Radio Meteorology," National Bureau of Standards, Monograph 92, p. 11, 1966.
5. Hopfield, H. S., "Two-Quartic Tropospheric Refractivity Profile for Correcting Satellite Data," *J. Geophys., Res.*, Vol. 74, No. 18, pp. 4487–4499, 1969.
6. Berman, A. L., "A New Tropospheric Range Refraction Model," in *The Deep Space Network*, Space Programs Summary 37-65, Vol. II, pp. 140–153. Jet Propulsion Laboratory, Pasadena, Calif., Sept. 30, 1965.
7. Hopfield, H. S., "Tropospheric Range Error at the Zenith," Preprint for 14th Plenary Meeting, July 1971, The John Hopkins University, Baltimore, Md.
8. Chao, C. C., "Improved Estimation of the Parameters and Mapping Tables of Tropospheric Calibration for MM'71," IOM 391.3-352, May 1971 (JPL internal document).
9. Chao, C. C., "Past vs. Current Tropospheric Calibration in DPODP and the Proposed Modifications for Future Missions," IOM 391.3-475, Oct. 4, 1971 (JPL internal document).
10. Winn, F. B., "Media Calibration for Radio Metric (Doppler) Tracking Data," TM 391-215, July 22, 1971 (JPL internal document).

**Table 1. Errors in refractivity *N***

| Error Sources | Ratio of rms error in refractivity to refractivity[a] | |
|---|---|---|
| Equation (1) | 0.5% | (1.6)[b] |
| Surface observations ($\pm$ 1 mb, $\pm$ 0.1°C, $\pm$ 1% *RH*) | 0.2% | (0.65) |
| Radiosonde observations ($\pm$ 2 mb, $\pm$ 1°C, $\pm$ 5% *RH*) | 1.3% | (4.2) |

[a] $P = 1013$ mb, $T_c = 15$°C, $RH = 60$%
[b] Terms in parentheses are $\Delta N$.

**Table 2. Radiosonde balloon site parameters**

| Radiosonde station | Elevation, m | Distance from nearest DSS, km | Nearest DSS | DSS elevation, m |
|---|---|---|---|---|
| Edwards AFB | 724 | 100 | Goldstone DSCC | 1032 |
| Yucca Flats | 1190 | 200 | Goldstone DSCC | 1032 |
| Madrid | 606 | 70 | Madrid DSCC | 789 |
| Wagga | 214 | 140 | Tidbinbilla DSCC | 656 |
| Woomera | 165 | 12 | Woomera | 151 |
| Pretoria | 1330 | 50 | Johannesburg | 1398 |

**Table 3. Monthly mean and standard deviation of dry refractivity at various altitudes above Edwards Air Force Base**

| Month | Dry refractivity, mean ($1\sigma$) | | | | | | | | |
|---|---|---|---|---|---|---|---|---|---|
| | Surface 0.72 km (2375 ft) | 3.66 km (12,000 ft) | 6.70 km (22,000 ft) | 9.75 km (32,000 ft) | 12.8 km (42,000 ft) | 15.8 km (52,000 ft) | 18.9 km (62,000 ft) | 25.0 km (82,000 ft) | 31.1 km (102,000 ft) |
| Jan | 262.4 | 187.9 | 136.9 | 97.3 | 63.6 | 40.1 | 24.4 | 8.8 | 3.2 |
| | (6.18) | (2.83) | (1.20) | (1.41) | (2.56) | (1.77) | (0.98) | (0.18) | (0.15) |
| Feb | 260.4 | 188.4 | 136.8 | 96.9 | 62.3 | 39.5 | 24.2 | 8.8 | 3.2 |
| | (3.86) | (1.85) | (0.81) | (1.96) | (1.78) | (1.03) | (0.38) | (0.08) | (0.05) |
| Mar | 255.8 | 187.2 | 136.1 | 96.9 | 62.7 | 39.4 | 24.0 | 8.6 | 3.3 |
| | (5.52) | (1.70) | (0.96) | (1.42) | (1.98) | (0.92) | (0.42) | (1.65) | (0.69) |
| Apr | 254.6 | 186.5 | 135.8 | 96.3 | 63.4 | 39.6 | 24.3 | 8.9 | 3.1 |
| | (4.57) | (1.63) | (1.26) | (1.65) | (1.86) | (0.83) | (0.42) | (0.07) | (0.79) |
| May | 249.7 | 185.3 | 135.5 | 96.7 | 64.0 | 39.8 | 24.4 | 9.0 | 3.5 |
| | (7.37) | (3.90) | (2.42) | (2.06) | (2.42) | (1.24) | (0.79) | (0.24) | (0.09) |
| June | 246.1 | 183.9 | 135.2 | 96.2 | 65.3 | 42.1 | 25.0 | 9.3 | 3.6 |
| | (2.87) | (1.90) | (1.27) | (2.15) | (1.71) | (1.39) | (0.82) | (0.30) | (0.16) |
| July | 243.2 | 182.2 | 134.3 | 95.5 | 67.3 | 44.6 | 26.2 | 9.6 | 3.7 |
| | (1.97) | (0.92) | (0.60) | (4.65) | (2.18) | (2.47) | (3.20) | (1.06) | (0.38) |
| Aug | 241.1 | 182.3 | 134.5 | 93.4 | 64.8 | 40.6 | 22.0 | 7.7 | 2.8 |
| | (3.78) | (0.84) | (0.56) | (0.78) | (1.21) | (0.95) | (0.64) | (1.37) | (0.66) |
| Sept | 246.7 | 184.3 | 133.9 | 96.6 | 65.9 | 42.7 | 25.4 | 8.7 | 3.4 |
| | (2.43) | (1.26) | (0.69) | (0.55) | (1.39) | (0.68) | (0.15) | (2.58) | (0.78) |
| Oct | 252.5 | 184.6 | 135.1 | 97.2 | 65.3 | 41.1 | 24.7 | 8.7 | 3.2 |
| | (5.50) | (1.68) | (1.16) | (0.57) | (1.17) | (0.75) | (0.31) | (1.85) | (0.90) |
| Nov | 255.0 | 184.4 | 134.9 | 96.9 | 65.9 | 41.2 | 24.6 | 8.9 | 3.1 |
| | (5.98) | (3.38) | (1.08) | (1.82) | (1.91) | (1.05) | (0.33) | (0.09) | (0.90) |
| Dec | 261.0 | 187.9 | 136.4 | 96.5 | 63.7 | 39.6 | 24.1 | 8.8 | 3.3 |
| | (4.56) | (1.84) | (0.98) | (1.39) | (1.97) | (0.70) | (0.32) | (0.06) | (0.04) |

**Table 4. Values of $N_W$ at different relative humidity and temperature**

| RH | 0°C | 10°C | 20°C | 30°C |
|---|---|---|---|---|
| 10% | 3.5 | 5.7 | 10.4 | 20.8 |
| 30% | 9.1 | 17.2 | 31.2 | 62.4 |
| 50% | 15.2 | 28.7 | 52.0 | 104.0 |
| 70% | 21.4 | 40.1 | 72.8 | 145.5 |

**Table 5. Summary of uncertainties ($1\sigma$) from monthly mean of wet refractivity at various altitudes for the six stations**

| Season | Surface | 1.83 km (6000 ft) | 3.66 km (12,000 ft) | 7.32 km (24,000 ft) |
|---|---|---|---|---|
| Summer months | 10 to 17 | 7 to 10 | 5 to 8 | 0.5 to 1.5 |
| Winter months | 4.5 to 9 | 3.5 to 7.5 | 2.5 to 6 | $< 0.5$ |

**Table 6. Uncertainties in tropospheric range correction (one-way) based on the two-year radiosonde balloon data (in meters)**

| $\gamma$ deg | $\sigma\Delta\rho_{dry}$ | | $\sigma\Delta\rho_{wet}$ | | $\sigma\Delta\rho_{total}$ | |
|---|---|---|---|---|---|---|
| | 2-Year | Monthly | 2-Year | Monthly | 2-Year | Monthly |
| 1 | 1.502 | 0.711 | 6.00 | 2.055 | 6.20 | 2.175 |
| 3 | 0.609 | 0.326 | 2.581 | 0.810 | 2.680 | 0.875 |
| 5 | 0.321 | 0.157 | 1.543 | 0.521 | 1.585 | 0.545 |
| 15 | 0.101 | 0.048 | 0.433 | 0.148 | 0.453 | 0.154 |
| 45 | 0.038 | 0.017 | 0.152 | 0.051 | 0.160 | 0.055 |
| 90 | 0.026 | 0.012 | 0.105 | 0.036 | 0.109 | 0.038 |

**Table 7. Comparison of zenith range correction at each DSS**

| Deep Space Station | Eq. 1, m | Eq. 2, m | Average from 2-year balloon measurement, m |
|---|---|---|---|
| Goldstone DSCC | 1.338 | 1.808 | $2.123 \pm 0.105$ |
| Madrid DSCC | 1.673 | 2.260 | $2.214 \pm 0.110$ |
| Woomera DSS | 1.895 | 2.562 | $2.374 \pm 0.118$ |
| Tidbinbilla DSCC | 1.729 | 2.336 | $2.259 \pm 0.111$ |
| Johannesburg DSS | 1.338 | 1.808 | $2.066 \pm 0.101$ |

**Table 8. Values of the uncertainty over one symmetrical pass in tropospheric range correction**

| Tracking station | From Eq. (17) | | From Eq. (18) | | New model (monthly mean) | |
|---|---|---|---|---|---|---|
| | Lowest elevation | | | | | |
| | 10 deg | 6 deg | 10 deg | 6 deg | 10 deg | 6 deg |
| Goldstone DSCC | 4.76 | 6.25 | 2.08 | 2.65 | 0.32 | 0.45 |
| Madrid DSCC | 3.57 | 4.59 | 0.85 | 1.05 | 0.34 | 0.47 |
| Woomera DSS | 2.87 | 3.77 | 1.40 | 1.74 | 0.31 | 0.43 |
| Tidbinbilla DSCC | 3.18 | 4.24 | 0.89 | 1.12 | 0.32 | 0.45 |
| Johannesburg DSS | 4.21 | 5.55 | 1.68 | 2.11 | 0.31 | 0.43 |

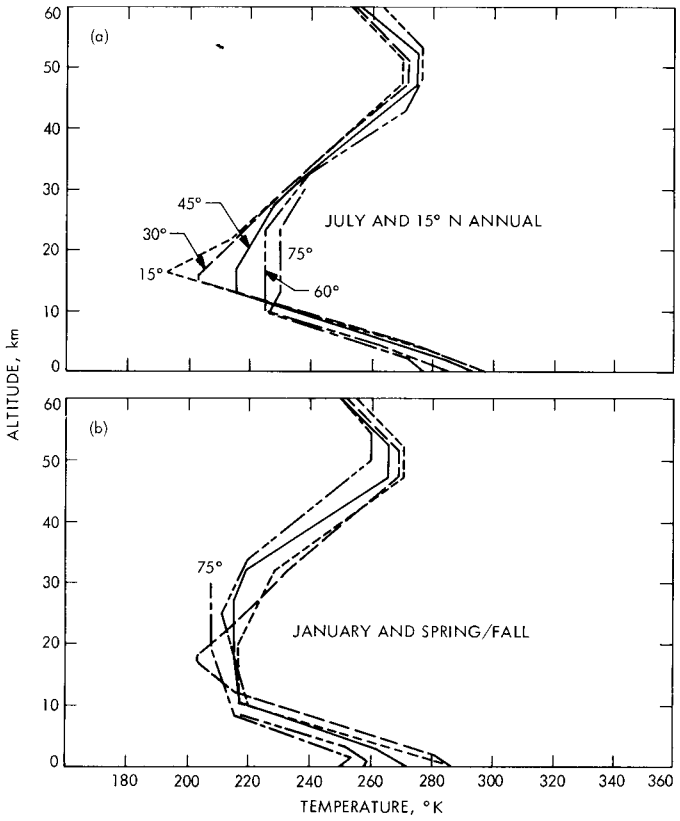


**Fig. 1. Temperature-altitude profiles of the 30, 45, 60 and 75 deg N (a) July and 15 deg N mean annual Supplementary Atmospheres, (b) January and midlatitude spring/fall Supplementary Atmospheres (from the U.S. Standard Atmosphere Supplements, 1966)**

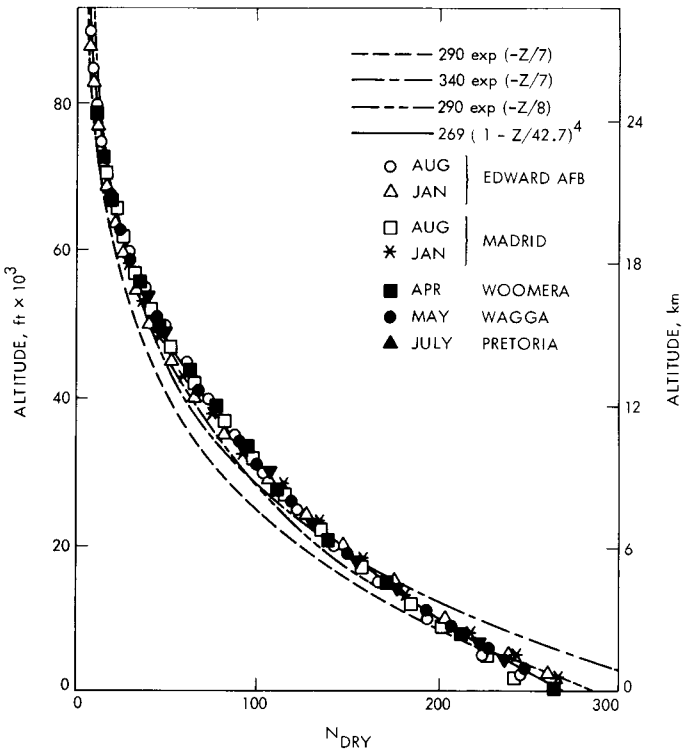


**Fig. 2. Dry refractivity profiles**

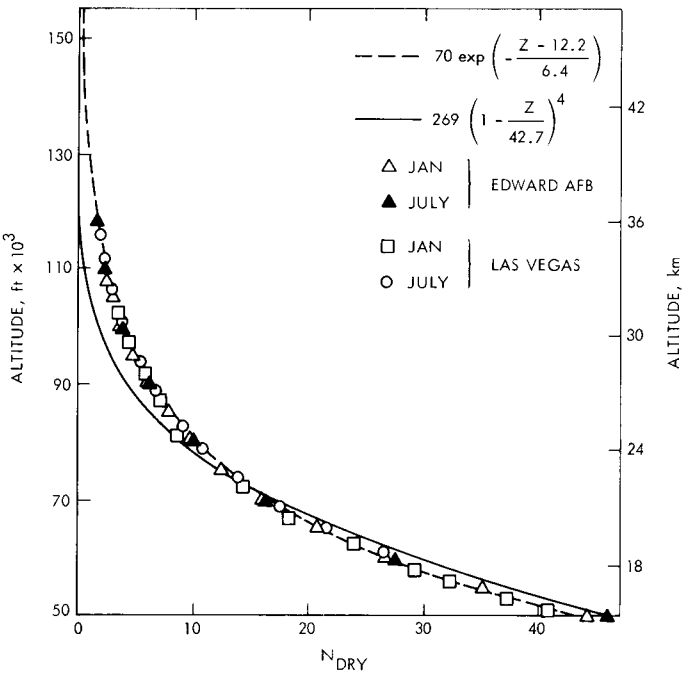


**Fig. 3. Dry refractivity profiles for altitudes higher than 15.3 km (50,000 ft)**

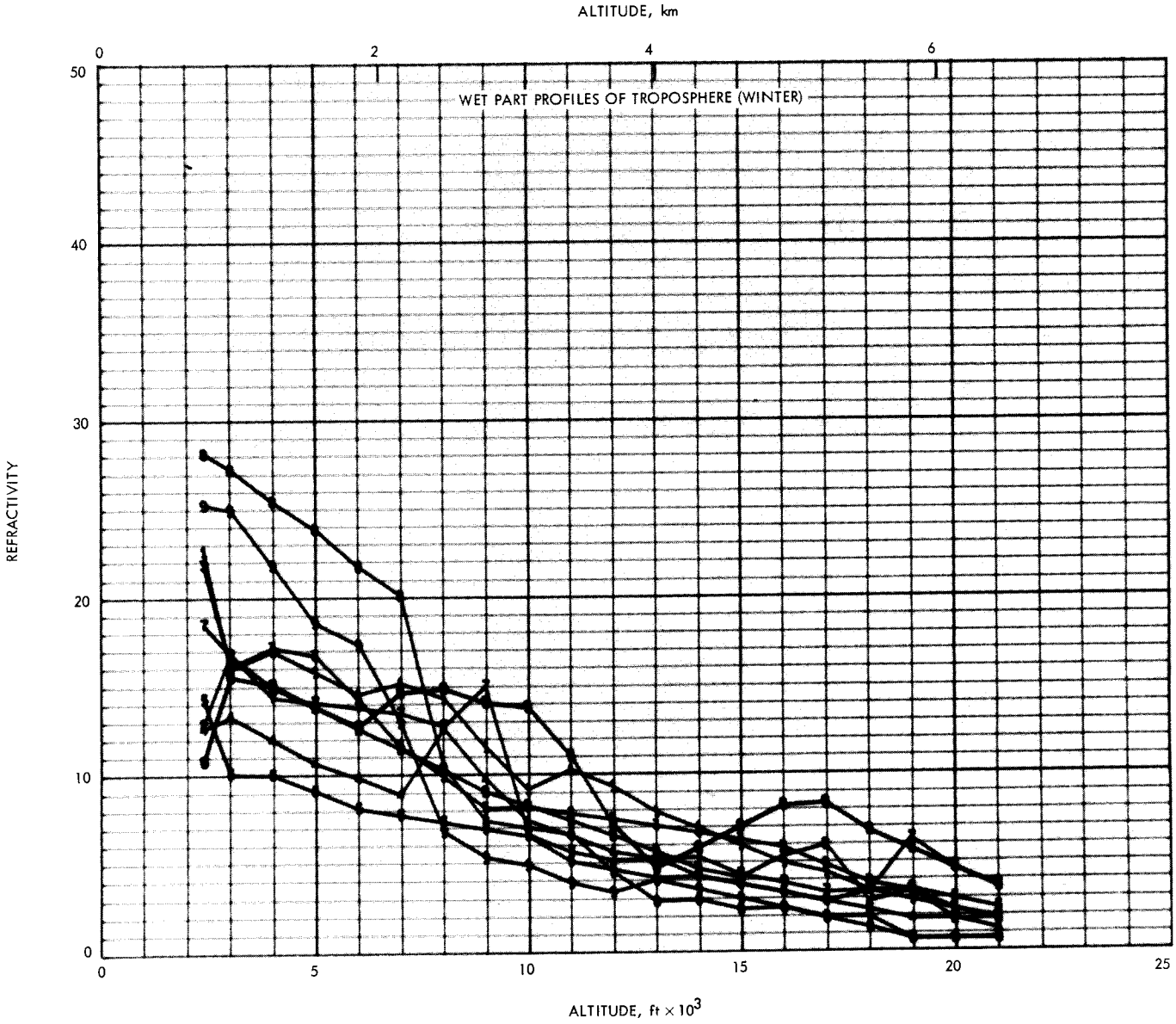


**Fig. 4. Wet refractivity profiles for Edwards A.F.B. in January, 1967**

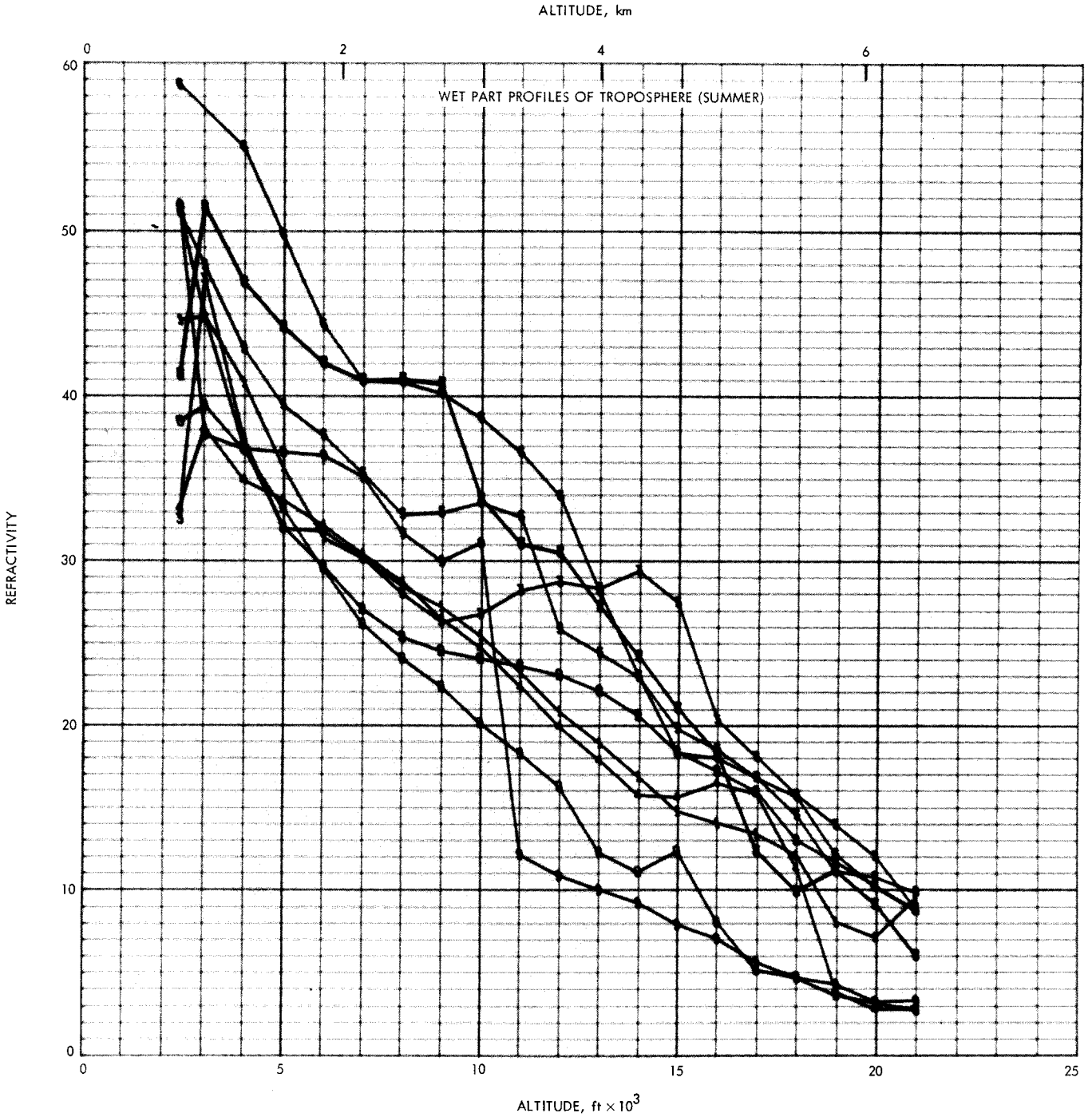


**Fig. 5. Wet refractivity profiles for Edwards A.F.B. in July, 1967**

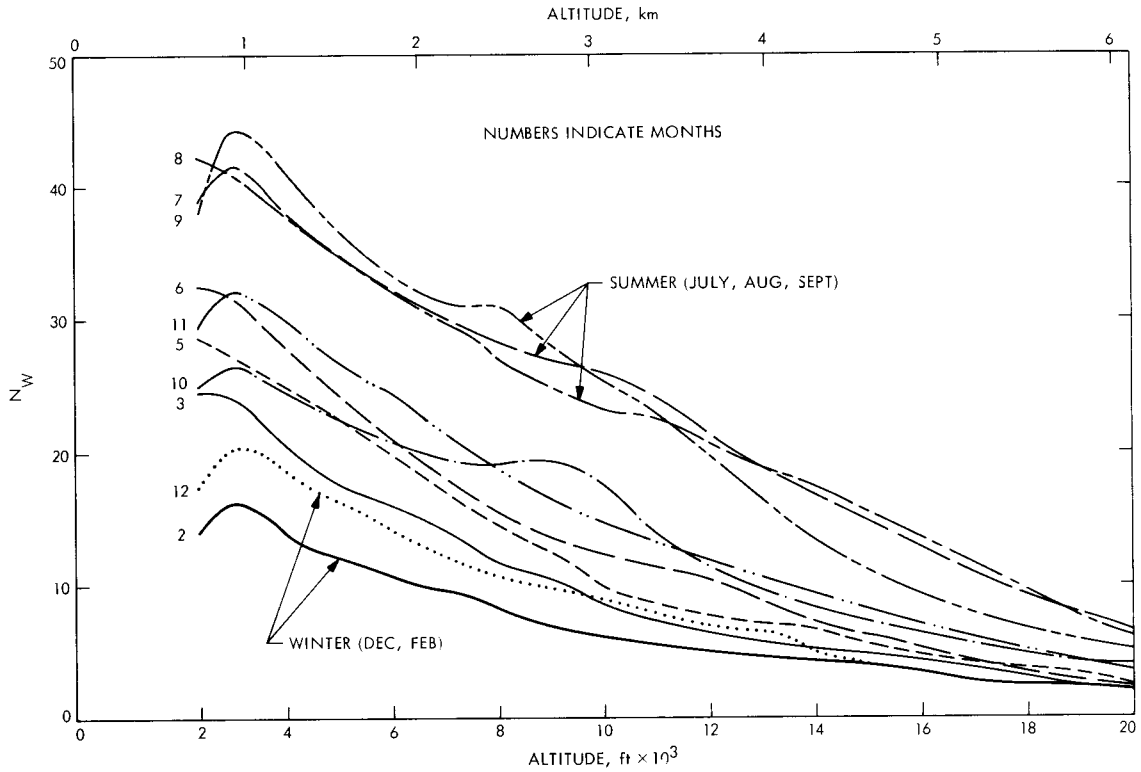


**Fig. 6. Monthly mean profiles of wet refractivity, Edwards A.F.B.**

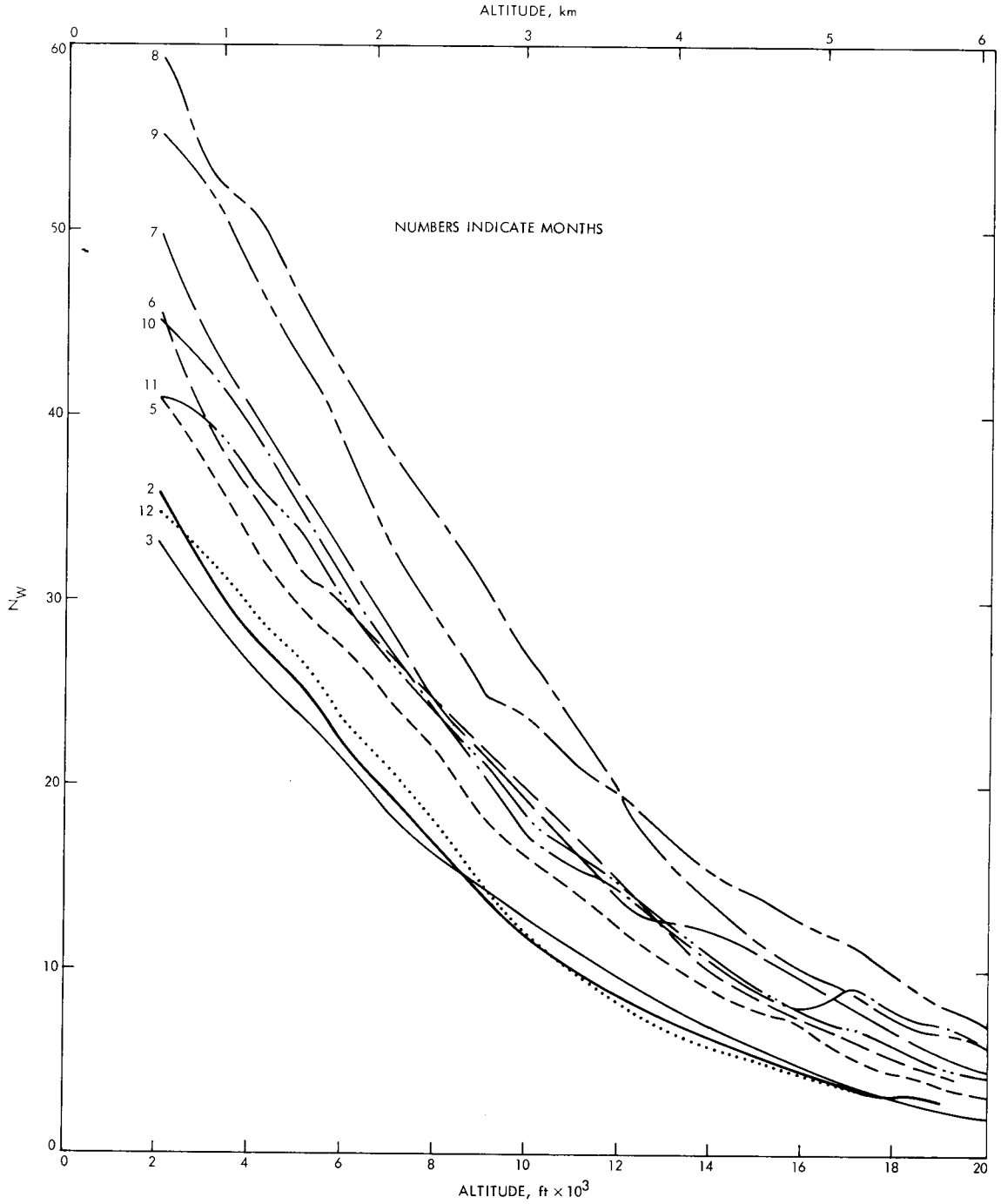


**Fig. 7. Monthly mean profiles of wet refractivity, Madrid**

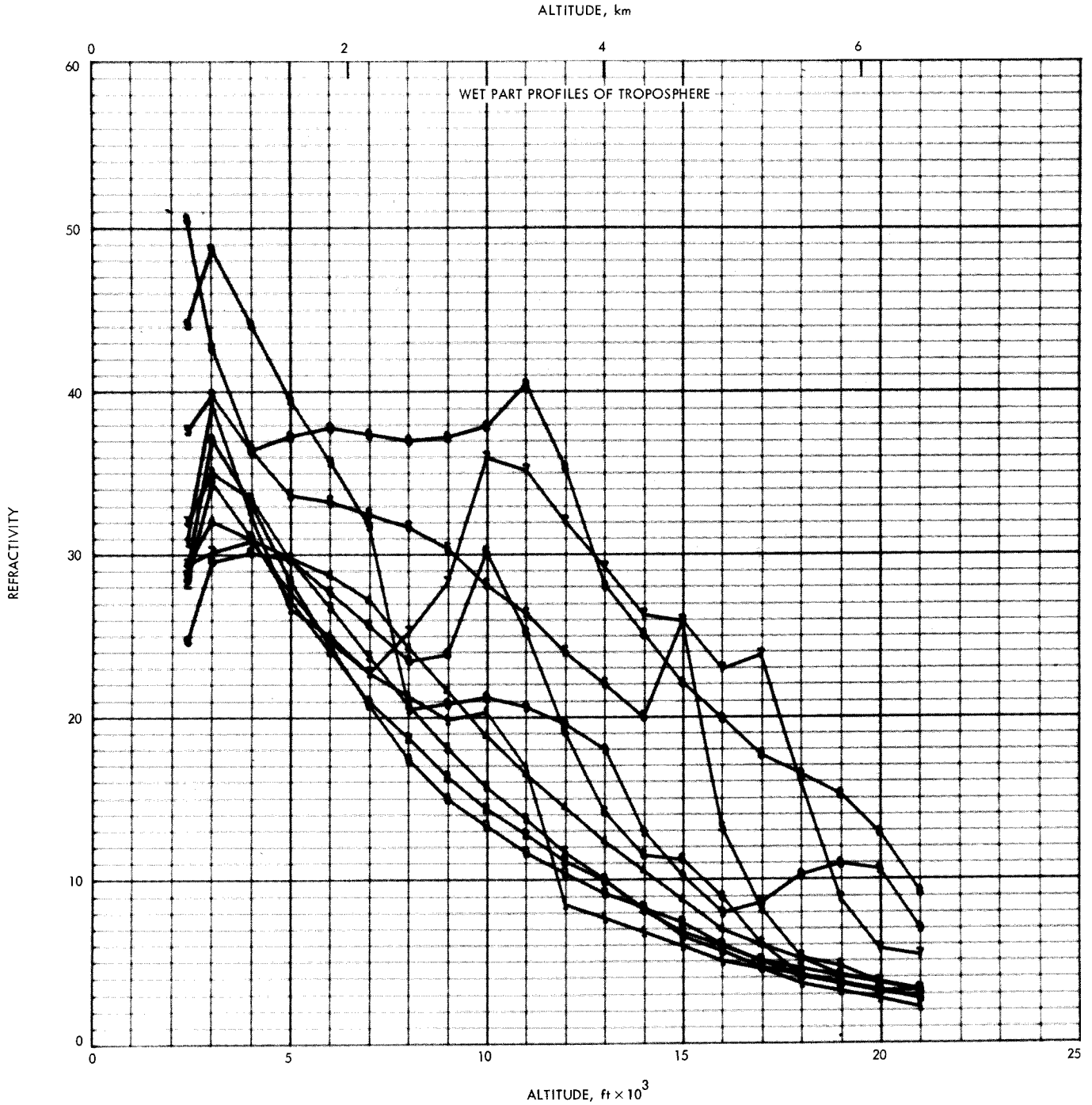


**Fig. 8. Wet refractivity profiles for Edwards A.F.B. in January, 1968**

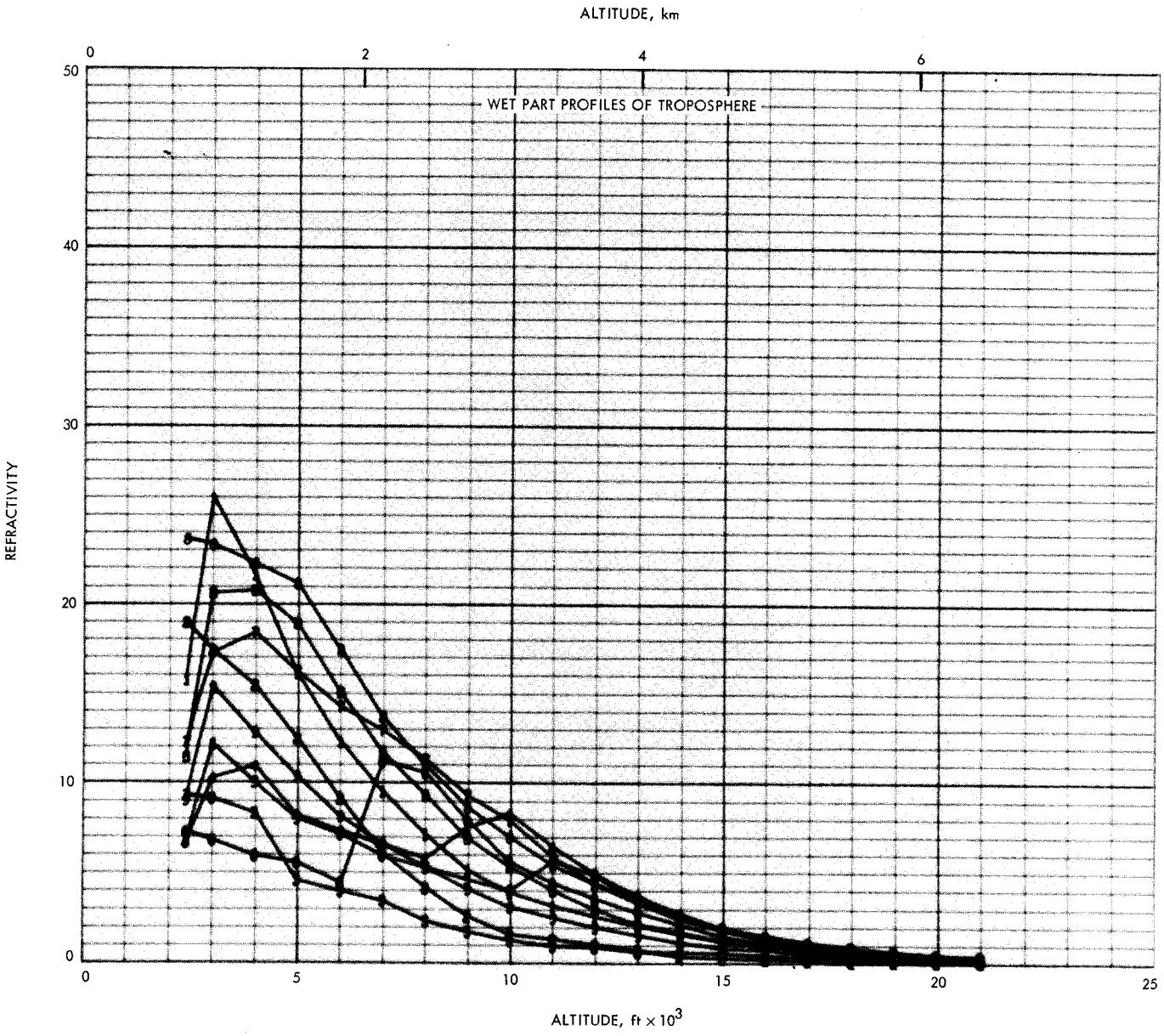


**Fig. 9. Wet refractivity profiles for Edwards A.F.B. in July, 1968**